Tunable Magnetic Trap: Using Passive Elements to Control Magnetic Microrobots

Franco N. Piñan Basualdo, Robert van de Weerd, and Sarthak Misra, *Senior Member, IEEE*

***Abstract*—Magnetic microrobots have the ability to navigate through difficult-to-reach environments, thereby holding promise for applications in the fields of micromanipulation and biomedicine. The actuation of these microrobots requires the generation and control of magnetic fields and gradients. However, the decay of gradients with the distance the (d) from the magnetic source (as $1/d^4$), poses challenges in generating gradients using remote sources. A possible solution is to use miniaturized magnetic sources that can be positioned closer to the microrobot. However, the small size of miniature magnetic sources limits the fields that can be generated. In this study, we propose a tunable magnetic trap—a system that combines remote magnetic field generation and local passive gradient generation. The remote field generation is achieved by a traditional Helmholtz system while gradients are generated locally by an arrangement of ferrite rods. The system benefits from strong external electromagnets and local gradient generation. The magnitude and direction of the magnetic gradient can be regulated with the external field, enabling the actuation of particles in the magnetic trap. The proposed system is validated experimentally through the control of a magnetic particle floating on the air-water interface. Our results show that relatively low magnetic fields ($<$5 mT) are necessary to displace a 500 μm metallic particle against the meniscus capillary force.**

***Index Terms*—Automation at Micro-Nano Scales, Micro/Nano Robots, Motion Control.**

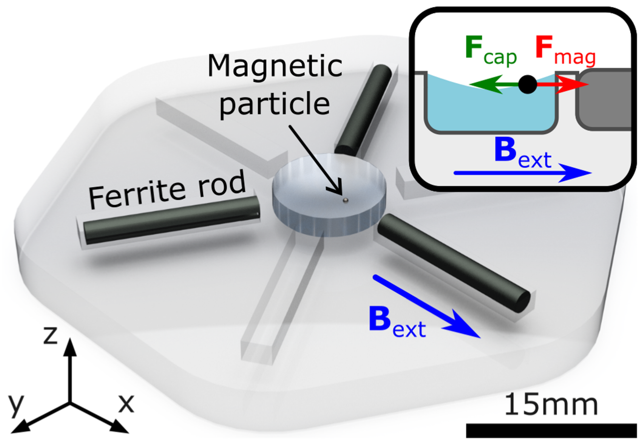

Fig. 1. Schematic of the tunable magnetic trap: The system consists of an arrangement of three ferrite rods that locally shape the magnetic field for the control of a particle in the center. The involved forces are shown in the inset. In a homogeneous magnetic field ($\mathbf{B}_{\text{ext}}$), the ferrite rods get magnetized inhomogeneously, giving rise to a magnetic force ($\mathbf{F}_{\text{mag}}$). Since the particle is on top of a fluid layer, there is also a capillary force ($\mathbf{F}_{\text{cap}}$) due to the meniscus shape.

I. Introduction

UNTETHERED microrobots have the ability to navigate through difficult-to-reach environments and perform precise tasks, holding promise for micromanipulation [1] and biomedical applications [2]. As a result, researchers are actively developing untethered microrobots, with advances in fabrication [3], tracking [4], and control [5]. Since embarking energy sources and computing units on microrobots can be technologically challenging, most untethered microrobots rely on external signals for actuation and control. Among the different actuation mechanisms, magnetic microrobots are the predominant ones, especially for biomedical applications [6]. Magnetic microrobots leverage magnetic fields for precise manipulation and control, enabling remote navigation within complex environments. We distinguish two main magnetic actuation strategies: Field- and gradient-based actuation [7].

Field-based magnetic microrobots exhibit motion as an indirect result of their interaction with the applied magnetic field and with the environment. The applied field, often homogeneous, does not generate considerable net forces. Instead, it is the microrobot's response to this field (rotation or deformation) that leads to its displacement. We identify three main types of field-based magnetic microrobots: Rollers, swimmers, and soft magnetic microrobots. Rollers are magnetic agents that, under a rotating field, roll on a surface to propel themselves, exploiting friction forces [8], [9]. Swimmers are magnetic agents, typically helical [10] or flagellar-shaped [11], that exhibit a swimming motion under a time-varying magnetic field, exploiting hydrodynamic forces. Finally, soft magnetic microrobots [12] deform under a magnetic field, which can result in varied locomotion modes (e.g, crawling [13], walking [14], and swimming [15]).

Gradient-based magnetic microrobots, on the other hand, are propelled by harnessing magnetic forces. A magnetic particle

Manuscript received 19 July 2023; accepted 8 December 2023. Date of publication 4 January 2024; date of current version 16 January 2024. This letter was recommended for publication by Associate Editor Jiangfan Yu and Editor Xinyu Liu upon evaluation of the reviewers' comments. This work was supported by the European Commission under the Horizon Europe program under Grant 101070066 (REGO). *(Corresponding author: Franco N. Piñan Basualdo).*

Franco N. Piñan Basualdo and Robert van de Weerd are with the Surgical Robotics Laboratory, Department of Biomechanical Engineering, University of Twente, 7522NB Enschede, The Netherlands (e-mail: f.n.pinanbasualdo@utwente.nl; g.j.vandeweerd@student.utwente.nl).

Sarthak Misra is with the Surgical Robotics Laboratory, Department of Biomechanical Engineering, University of Twente, 7522NB Enschede, The Netherlands, and also with the Surgical Robotics Laboratory, Department of Biomaterials and Biomedical Technology, University of Groningen and University Medical Centre Groningen, 9713 GZ Groningen, The Netherlands (e-mail: s.misra@utwente.nl).

This letter has supplementary downloadable material available at https://doi.org/10.1109/LRA.2024.3349810, provided by the authors.

Digital Object Identifier 10.1109/LRA.2024.3349810

in a non-homogeneous magnetic field will be attracted to areas of stronger magnetic field [7] (i.e., in the direction of the magnetic gradient). Gradient-based actuation can achieve precise movements [16], [17] and it can enable the simultaneous control of multiple microrobots [18], [19]. Moreover, gradient-based position control can be combined with field-based orientation control for complete pose control, opening the way to advanced tasks like cargo transport [12], [20].

The control of gradient-based microrobots is typically achieved using electromagnetic systems [21]. These systems control the magnetic field and gradient by adjusting the currents circulating through a set of electromagnetic coils that surround the workspace. These coils can be air-core coils, which respond linearly and can be actuated at high frequencies [22]. However, iron-core coils are frequently preferred (despite the associated non-linearities and increased inductance) for their stronger effect [23], [24], [25]. One limitation of gradient-based systems is that the generated magnetic gradient decreases with the distance (d) from the electromagnet as $1/d^4$. Therefore, the remote generation of magnetic gradients requires strong coils, which would consume more energy.

An alternative approach is to use miniature electromagnets positioned in the proximity of the workspace to minimize the distance from the electromagnets [26], [27], [28]. However, the heat generated by the coils is dissipated close to the workspace, which can be harmful for the manipulation of sensitive components. Therefore, the supply power, and thus the magnetic field and gradient, must be limited. In this work, we introduce a tunable magnetic trap, a hybrid magnetic actuation system combining active-external and passive-local magnetic actuation, which results in no heat dissipation in the workspace vicinity.

The proposed tunable magnetic trap consists of the generation of magnetic fields using external Helmholtz coils and a local arrangement of passive ferrite rods. The homogeneous magnetic field generated by the coils would not give place to magnetic forces by itself. However, the ferrite rods locally concentrate the field, producing a trap that attracts magnetic particles [29]. By arranging the ferrite rods appropriately, we can generate a dependence of the resulting trapping force with the applied field—thus resulting in a tunable magnetic trap. Thereby, a magnetic particle in the trap can be controlled by only adjusting the externally applied magnetic field. One advantage of the proposed hybrid system is that the external electromagnetic coils can generate stronger fields than miniature coils and that the heat is dissipated outside the workspace. Moreover, the local effect of the ferrite rods generates higher gradients than purely external systems. The effectiveness of the proposed system is demonstrated experimentally through the closed-loop control of a magnetic particle of $500\,\mu\text{m}$, which required the application of relatively weak fields (<5 mT) due to the proximity of the ferrite rods.

II. Actuation

The proposed actuation system is based on the anisotropic magnetization of ferrite rods for the creation of a tunable magnetic trap. A magnetic particle inside the trap experiences a net force that can be controlled (in both magnitude and direction) by varying the applied external magnetic field.

A. Principle

The proposed tunable magnetic trap consists of Helmholtz coils and an arrangement of ferrite rods for the manipulation of magnetic particles, as shown in Fig. 1. The Helmholtz coils system generates homogeneous fields in the workspace, which normally would not result in magnetic forces. Under this external magnetic field ($\mathbf{B}_{\text{ext}}$), the ferrite rods get magnetized, locally strengthening the magnetic field and creating a magnetic trap. In the case of anisotropic magnetic components, the magnetization strength depends on the relative orientation of the magnetic field. For ferrite rods, the material can be considered isotropic, but its elongated shape (aspect ratio 7.5) gives place to a highly anisotropic magnetization. Notably, when the field is aligned with the rod, the magnetization is up to 20 times higher than when the field is perpendicular to the rod, as shown in Fig. 2. This anisotropic magnetization of the ferrite rods makes it possible to tune the magnetic trapping by controlling the magnetic field direction and magnitude.

The proposed configuration (three ferrite rods arranged symmetrically around a circular workspace) gives place to a 2D tunable magnetic trap. The ferrite rod magnetization depends on their orientation relative to the applied external field ($\mathbf{B}_{\text{ext}}$). Therefore, a magnetic gradient surges in between the rods, whose direction depends on the applied external field. For example, an external field in the $+x$ direction generates a gradient also in the $+x$ direction, and an external field in the $+y$ direction generates a gradient in the $-x$, as shown in Fig. 3.

Notice that since the magnetization of the ferrite rods depends only on the relative magnetic field orientation, the gradient generated by any $\mathbf{B}_{\text{ext}}$ and its inverse ($-\mathbf{B}_{\text{ext}}$) are the same. Moreover, due to the system's three-fold symmetry, these results can be extrapolated to the other rods by rotating the frame of reference.

B. Modeling

The three forces acting on a magnetic particle in the interior of a tunable magnetic trap are the magnetic force ($\mathbf{F}_{\text{mag}}$), the capillary force ($\mathbf{F}_{\text{cap}}$), and the drag force ($\mathbf{F}_{\text{drag}}$).

Magnetic forces: The magnetic force experienced by a soft magnetic particle can be estimated using the dipole model [25]:

$$\mathbf{F}_{\text{mag}} = \frac{\chi_{\text{eff}} V}{\mu_0} \nabla \|\mathbf{B}\|^2 = 2\,\frac{\chi_{\text{eff}} V}{\mu_0}\,\mathbf{J}_B^T \times \mathbf{B}, \tag{1}$$

where χ_{eff} is the effective magnetic susceptibility, V is the particle volume, μ_0 is the vacuum magnetic permeability, $\mathbf{B}$ is the magnetic field, and $\mathbf{J}_B$ is the Jacobian of the magnetic field. The effective magnetic susceptibility depends on the material and shape of the particle [30]. For the particular case of a magnetic sphere, we get $\chi_{\text{eff}} \approx 3$.

In the proposed tunable magnetic trap, both the field and its Jacobian in the interior depend linearly on the applied magnetic

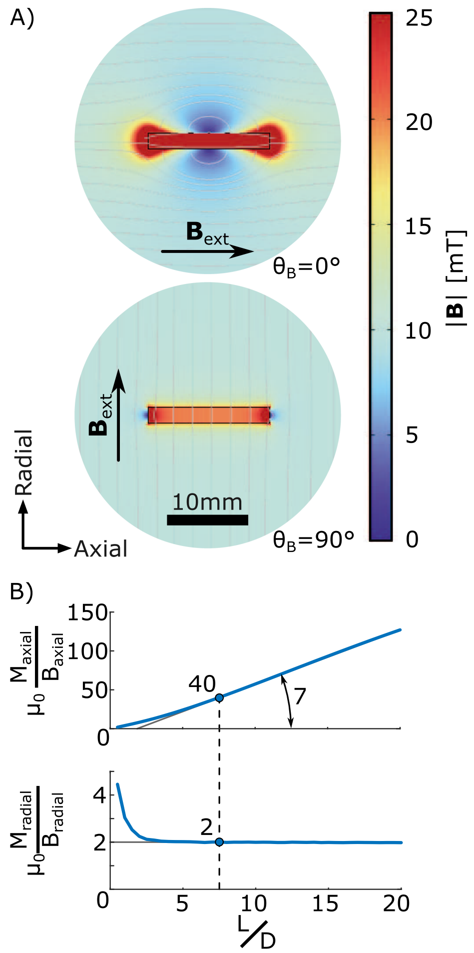

Fig. 2. Finite element simulations results of the magnetization ($\mathbf{M}$) of a single ferrite rod in an external homogenous field ($\mathbf{B}_{\text{ext}}$). A) Magnetization of a rod (diameter $D = 2\,\text{mm}$, length $L = 15\,\text{mm}$, relative permeability $\mu_r = 2300$, $\|\mathbf{B}_{\text{ext}}\| = 10\,\text{mT}$) and resulting magnetic field ($\mathbf{B}$) for the aligned ($\theta_B = 0^\circ$) and perpendicular ($\theta_B = 90^\circ$) cases. B) Non-dimensional axial and radial magnetization ($\mu_0\,\mathbf{M}/\|\mathbf{B}_{\text{ext}}\|$, where μ_0 is the vacuum magnetic permeability) at the center of the rod as a function of the aspect ratio (L/D) of the rod. For large aspect rations ($L/D > 5$), the axial magnetization becomes dominant.

field ($\mathbf{B}_{\text{ext}}$):

$$\begin{cases} \mathbf{B} = B_{\text{ext}_x}\,\tilde{\mathbf{B}}_x + B_{\text{ext}_y}\,\tilde{\mathbf{B}}_y \\ \mathbf{J}_B = B_{\text{ext}_x}\,\tilde{\mathbf{J}}_x + B_{\text{ext}_y}\,\tilde{\mathbf{J}}_y, \end{cases} \tag{2}$$

where B_{ext_x}, B_{ext_y} are components of the external field, and ($\tilde{\mathbf{B}}_x$, $\tilde{\mathbf{B}}_y$) and ($\tilde{\mathbf{J}}_x$, $\tilde{\mathbf{J}}_y$) are the resulting fields and Jacobian when a unit external field is applied in the x or y direction, respectively. Therefore, the tunable magnetic trap can be fully characterized by its response to a unit field in each direction. Then, equations (1) and (2) can be used to compute the resulting force for any applied magnetic field.

In the case of the symmetric arrangement of three ferrite rods, the expression for the force at the center of the workspace can be further simplified. The numerical simulations, shown in Fig. 3, are used to compute ($\tilde{\mathbf{B}}_x$, $\tilde{\mathbf{B}}_y$) and ($\tilde{\mathbf{J}}_x$, $\tilde{\mathbf{J}}_y$). In this case, the gradient orientation is found to be -2 times the orientation of the applied external field, which enables the simplification of (1) to:

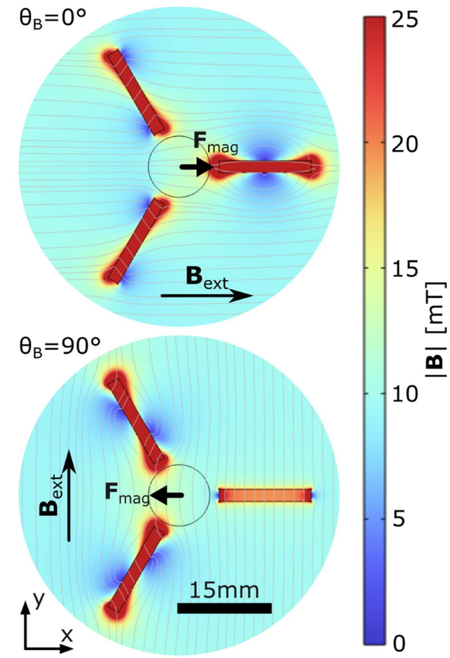

Fig. 3. Resulting magnetic field ($\mathbf{B}$) in an arrangement of three ferrite rods ($2\,\text{mm}$ diameter, $15\,\text{mm}$ long, relative permeability 2300) under an external homogeneous field ($\mathbf{B}_{\text{ext}}$) of $10\,\text{mT}$. Finite element simulation results for fields applied in the x or y direction. The direction of the magnetic gradient (and thus, the force) depends non-linearly on the orientation of the external magnetic field.

$$\begin{cases} \|\mathbf{F}_{\text{mag}}\| = \dfrac{\chi_{\text{eff}} V}{\mu_0\, L_F} \|\mathbf{B}_{\text{ext}}\|^2 \\ \theta_F = -2\theta_B, \end{cases} \tag{3}$$

where L_F is a length that depends on the arrangement of ferrite rods, and θ_B and θ_F are the orientation of the magnetic field and force, respectively.

Capillary forces: Due to the meniscus concave shape, a heavy particle floating on the interface will tend towards the center of the workspace. This capillary force ($\mathbf{F}_{\text{cap}}$) can be modeled as: [31]

$$\mathbf{F}_{\text{cap}} = -\frac{mg}{R_c}\mathbf{P}, \tag{4}$$

where m is the particle mass, g is the gravity acceleration, R_c is the meniscus curvature, and $\mathbf{P}$ is the particle position with respect to the center of the recipient.

Drag force: The last force to consider is the drag force acting on the particle. The drag force results from the viscosity of the fluid and tends to slow down the particle. Since in our case the particle is not completely submerged, we model the drag force with a generalized Stokes' Law:

$$\mathbf{F}_{\text{drag}} = -b_d\,\dot{\mathbf{P}}, \tag{5}$$

where b_d is the drag coefficient, which depends on the fluid and particle properties.

Finally, combining (1), (4), and (5), the system dynamics can be modeled as

$$m\,\ddot{\mathbf{P}} + b_d\,\dot{\mathbf{P}} + \frac{mg}{R_c}\mathbf{P} = \mathbf{F}_{\text{mag}}. \tag{6}$$

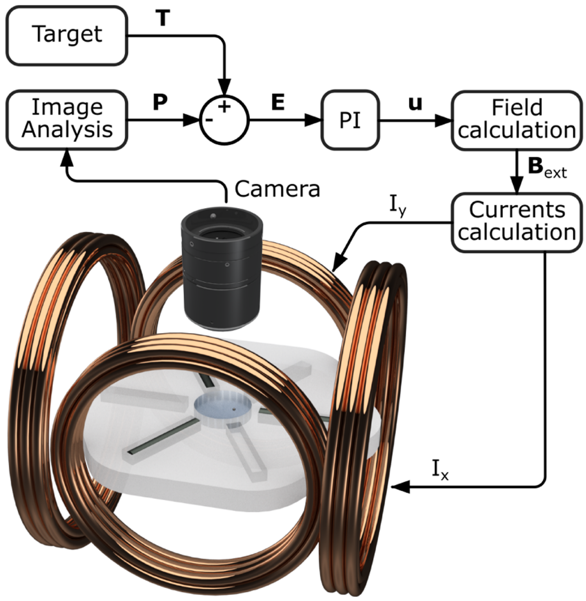

Fig. 4. Closed-loop control diagram. The camera view of the workspace is used to compute the particle position (**P**). The error (**E**) with respect to the target position (**T**) is fed to the Proportional-Integral controller to compute the required control (**u**) using (10). Then, (8) is used to determine the required magnetic field ($\mathbf{B}_{\text{ext}}$). Finally, the required currents the I_x and I_y are computed and sent to the Helmholtz system (here represented out of scale).

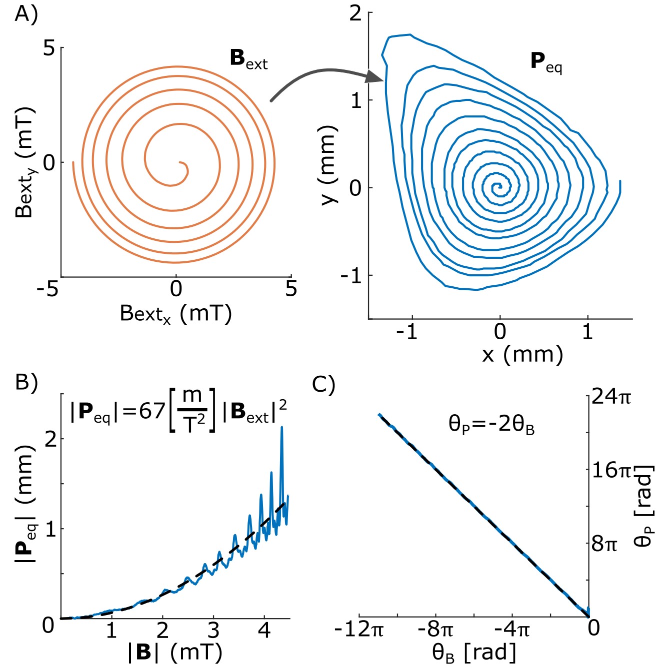

Fig. 5. Experimental system response to a quasistatic input. The equilibrium position is measured as a function of the applied external field. A) A spiral in the magnetic field ($\mathbf{B}_{\text{ext}}$) is applied (left) and the resulting equilibrium position of the particle ($\mathbf{P}_{\text{eq}}$) is measured (right). B) Distance from the center as a function of the applied magnetic field intensity. We fitted a quadratic function $\|\mathbf{P}_{\text{eq}}\| = 67\,\mathrm{m}/\mathrm{T}^2\,\|\mathbf{B}\|^2$. The deviations from the quadratic model can be explained by the spatial variation of the generated magnetic gradient. C) The angle of the particle position (θ_P) as a function of the orientation of the applied magnetic field (θ_B). The measurements are in good agreement with the model $\theta_P = -2\,\theta_B$.

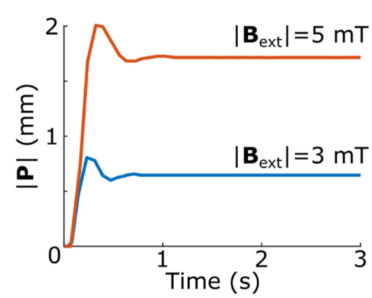

Fig. 6. Experimental dynamic characterization. The distance from the center ($\|\mathbf{P}\|$) response to a step increase in the applied magnetic field ($\mathbf{B}_{\text{ext}}$) is measured for a 3 mT and 5 mT step increase. The open-loop system settling time and overshoot are 1 s and 20 %, respectively.

According to (6), for a given external field, the particle will find its equilibrium at the point where the magnetic and capillary forces cancel each other. Using (3) to compute the magnetic force we find:

$$\begin{cases} \|\mathbf{P}_{\text{eq}}\| = \dfrac{\chi_{\text{eff}}\, V\, R_c}{\mu_0\, L_F\, mg} \|\mathbf{B}_{\text{ext}}\|^2 \\ \theta_P = -2\theta_B, \end{cases} \tag{7}$$

where θ_P is the orientation of the equilibrium position with respect to the center of the workspace.

C. Control Strategy

To compensate for modeling errors (e.g, our model does not consider spatial variations of the gradient) and experimental conditions variation (e.g, changes in the meniscus curvature due to contact angle hysteresis), we developed a closed-loop controller. We define the field direction and magnitude by rewriting (3) as a function of a new control variable **u** as:

$$\begin{cases} \|\mathbf{B}_{\text{ext}}\| = \sqrt{\|\mathbf{u}\|} \\ \theta_B = -\frac{1}{2}\theta_u, \end{cases} \tag{8}$$

where θ_u is the orientation of **u**. Substituting (8) in (3) and (6) we obtain:

$$m\,\ddot{\mathbf{P}} + b_d\,\dot{\mathbf{P}} + \frac{mg}{R_c}\mathbf{P} = \frac{\chi_{\text{eff}} V}{\mu_0\, L_F}\,\mathbf{u}. \tag{9}$$

Finally, we define our controller as a proportional-integral (PI) controller:

$$\mathbf{u} = K_P\,\mathbf{E} + K_I \int_0^t \mathbf{E}\,dt, \tag{10}$$

where **T** is the target position, $\mathbf{E} = \mathbf{T} - \mathbf{P}$ is the error, and K_P and K_I are the proportional and integral gains, respectively.

III. Experimental Validation

The proposed actuation system and control strategies are validated experimentally by controlling the movement of a soft magnetic particle floating on the air-water interface.

A. Experimental Implementation

Experimentally, we utilized an arrangement of orthogonal Helmholtz coil pairs, previously introduced by Thomas et al., to

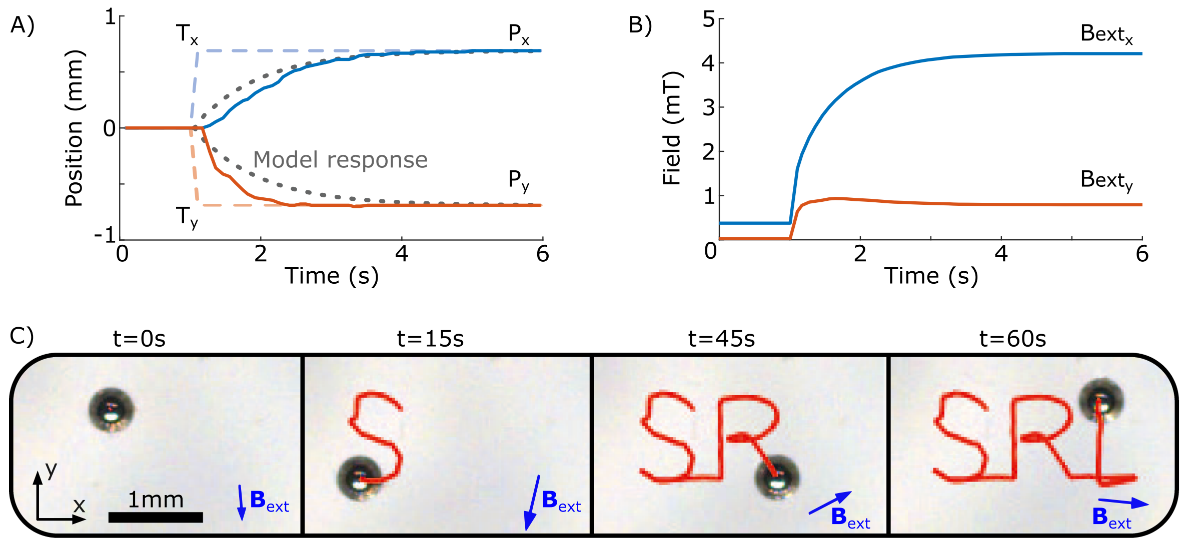

Fig. 7. Experimental closed-loop control results. A) System response to a step increase in the target position. The solid lines represent the particle position ($\mathbf{P} = (P_x, P_y)$), the dashed lines, the target ($\mathbf{T} = (T_x, T_y)$), and the dotted gray lines, the closed-loop dynamic model step response. The closed-loop system settling time is 3 s and the overshoot of the open-loop system, shown in Fig. 6, is eliminated. B) Externally applied magnetic field ($\mathbf{B}_{\text{ext}} = (B_{\text{ext}_x}, B_{\text{ext}_y})$) evolution corresponding to the transient response shown in the previous panel. C) Trajectory of the particle in a point-to-point control experiment writing the lab's initials 'SRL'. The red curve represents the particle's trajectory and the blue arrow is the applied external field ($\mathbf{B}_{\text{ext}}$). Please refer to Supplementary Video.

generate the required external magnetic field [32]. These coils generate a mostly homogeneous magnetic field of up to $55\,\text{mT}$ in any direction in a workspace of $65\,\text{mm}$. The arrangement of ferrite rods is placed in the center of the coil system, as shown in Fig. 4. Therefore, the direction and magnitude of the external magnetic field, and thus the resulting magnetic gradient, can be controlled by adjusting the currents circulating through each pair of coils.

The magnetic response of our particular arrangement of ferrite rods (three rods placed symmetrically at $6.5\,\text{mm}$ from a common center as shown in Fig. 3) is studied through finite element simulations in COMSOL Multiphysics (version 6.0, COMSOL, Inc, Sweden). By simulating the system response to different applied magnetic fields in the geometric center of the workspace we obtain:

$$\tilde{\mathbf{B}}_x = \begin{bmatrix} 1.16 \\ 0 \\ 0 \end{bmatrix} \qquad \tilde{\mathbf{J}}_x = \begin{bmatrix} 48 & 0 & 0 \\ 0 & -48 & 0 \\ 0 & 0 & 0 \end{bmatrix} \text{m}^{-1}$$

$$\tilde{\mathbf{B}}_y = \begin{bmatrix} 0 \\ 1.16 \\ 0 \end{bmatrix} \qquad \tilde{\mathbf{J}}_y = \begin{bmatrix} 0 & 48 & 0 \\ 48 & 0 & 0 \\ 0 & 0 & 0 \end{bmatrix} \text{m}^{-1}. \tag{11}$$

Replacing (11) in (2), we obtain (3) with $L_F = 9\,\text{mm}$. The controlled magnetic particle is an AISI 420 C stainless steel sphere of $500\,\mu\text{m}$ diameter. Although the magnetic response can be accurately modeled numerically, modeling the capillary and drag forces would require knowing precisely the meniscus curvature and the particle immersion depth on the interface. Since these magnitudes are difficult to measure and can vary between experiments (because of contact angle hysteresis), we estimate these values through experimental characterization.

B. Characterization

Two empirical characterization measurements are performed: Static and dynamic characterization. The static characterization, shown in Fig. 5, consists of varying the applied field (both in magnitude and direction) while measuring the position of the particle. Since the variation is slow (<2 mT/s), the particle can be considered to always be in equilibrium. Notice that when the applied field is weak (below $3\,\text{mT}$), the distance of the particle to the center is independent of the field orientation and quadratic with the field magnitude (as $\|\mathbf{P}_{\text{eq}}\| = 67\,\text{m}/\text{T}^2\,\|\mathbf{B}\|^2$). Using (7), we estimate a meniscus curvature of $R_c \approx 19\,\text{mm}$ (approximately twice the diameter of the water reservoir). On the other hand, when the applied field is strong (above $3\,\text{mT}$), there is a coupling between magnitude and orientation, which can be explained by the spatial variation of the magnetic forces. The dynamic characterization, shown in Fig. 6, consists of measuring the particle position response to a sudden increase in the applied magnetic field. By fitting a second-order model to these transient responses and comparing it with (6), we estimate $b_d \approx 10\,\text{mg/s}$. This value is twice as much as we would obtain using the Stokes' law, as it is known that partially submerged particles experience higher drag forces [33]. The open-loop system exhibits an overshoot of approximately $20\,\%$ and a settling time of $1\,\text{s}$. Therefore, we implement a closed-loop controller to compensate for unaccounted spatial variations of the magnetic force and enhance the system's transient response.

C. Closed-Loop Control

The control law (10) is implemented experimentally with gains $K_P = 0.7\,\text{mT}^2/\text{mm}$ and $K_I = 22\,\text{mT}^2/(\text{mms})$. The results are shown in Fig. 7. The empirical closed-loop step response is in good agreement with the developed dynamic model.

TABLE I
COMPARISON WITH OTHER ELECTROMAGNETIC ACTUATION SYSTEMS. WE COMPARE THE MAXIMUM MAGNETIC FIELD ($\|\mathbf{B}\|_{\text{MAX}}$) THAT CAN BE ATTAINED, THE GRADIENT-TO-FIELD RATIO ($\|\nabla\mathbf{B}\|/\|\mathbf{B}\|$), AND THE ACCESSIBLE WORKSPACE SIZE

	Factor	$\|\mathbf{B}\|$	$\frac{\|\nabla\mathbf{B}\|}{\|\mathbf{B}\|}$	Workspace
	Unit	[mT]	[m^{-1}]	[mm]
External	Open config. [34]	15	35	80
	Antiprism [35]	30	40	20
	OctoMag [23]	30	25	25
	BigMag [24]	40	25	100
	Toroidal [36]	50	5	70
	Maxwell [22]	100	15	60
	BatMag [25]	100	20	35
	CGCI [37]	100	8	150
Local	MiniMag [26]	20	100	10
	MILiMAC [27]	8	370	8
	MagNeed [28]	9	380	10
	μMAZE [38]	0.15	8000	13
Tunable trap		55	60	13

The closed-loop system exhibits a response with a settling time of 3 s and no overshoot, which is an improvement over the 20 % overshoot of the open-loop system. The robustness of the proposed controller is showcased by performing the point-to-point control of the particle. Furthermore, we use the particle's trajectory to describe 'SRL' (which are the initials of Surgical Robotics Laboratory) by changing the target once it has been reached. Despite the spatial variation of the magnetic force, the particle is successfully driven to different points of the workspace with negligible steady-state error.

IV. DISCUSSION

In this letter, we propose a tunable magnetic trap as a new kind of gradient-based magnetic actuation system, combining remote electromagnets and a local arrangement of ferrite rods. The remote electromagnets generate a homogeneous magnetic field within the workspace, while the ferrite rods generate local magnetic gradients. Due to the anisotropic magnetization of the rods, the magnetic gradient in the trap depends on the direction of the applied magnetic field, hence the name of a tunable magnetic trap. The capabilities of the system are validated through the closed-loop control of a soft magnetic particle floating on the air-water interface. Because of the proximity of the rods to the workspace, relatively weak magnetic fields (<5 mT) are necessary to generate a strong enough magnetic gradient to displace a 500 μm stainless steel particle against the meniscus capillary force.

We compare the proposed approach with both external and local magnetic actuation systems using the maximum magnetic field and gradient, as shown in Table I. Although in the proposed system, the applied magnetic field and the resulting gradient are inherently coupled (which would make the simultaneous position and orientation control difficult), it presents several advantages. The main benefit of the proposed approach is that the electromagnets, being external, can generate higher fields compared to miniature magnetic actuation systems, which would enable the control of weakly magnetic components. On the other hand, the local passive components can generate magnetic gradients that, for the same field, are stronger (from 50 % to 200 %) than purely external systems. Moreover, in the tunable magnetic trap case, the field-to-gradient map can be adjusted for a targeted application by displacing the ferrite rods. For example, approaching the three rods to the center would increase the generated gradient in a reduced workspace.

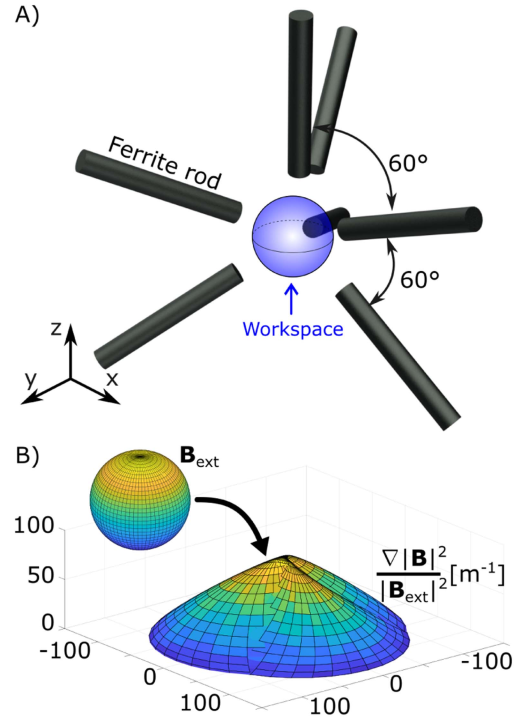

Fig. 8. 3D tunable trap concept. A) Proposed arrangement of ferrite for a 3D trap. The arrangement consists of one vertical rod on top of the workspace and three pairs of rods symmetrically distributed in the $x-y$ plane. B) Characteristic external field ($\mathbf{B}_{\text{ext}}$) to gradient ($\nabla\|\mathbf{B}^2\|$) map. A sphere in the field domain is mapped into a cone-like shape in the gradient domain. Notice that the gradient in the z direction is always positive.

The proposed approach of using local passive components for the generation of magnetic forces opens the way for future research directions. For example, the proposed system could be used to control multiple particles on the air-water interface exploiting magneto-capillary interactions [39]. This, however, would require considering the spatial variation of the magnetic gradients. On the other hand, the actuation principle can be extended to 3D manipulation using an arrangement of ferrite rods as the one shown in Fig. 8 in a 3D Helmholtz system. Although the gradient in the z direction is always upwards, it can be useful for levitating magnetic particles against gravity. Finally, a tunable magnetic trap could be used to sort magnetic particles in a microfluidic channel. Indeed, if the ferrite rods are placed around a tube in which a fluid with suspended magnetic particles circulates, then an external magnetic field could be used to steer the particles in the suspension in a controllable way.

REFERENCES

[1] M. A. Rahman and A. T. Ohta, "Micromanipulation with microrobots," *IEEE Open J. Nanotechnol.*, vol. 2, pp. 8–15, 2021.
[2] M. Sitti et al., "Biomedical applications of untethered mobile milli/microrobots," *Proc. IEEE*, vol. 103, no. 2, pp. 205–224, Feb. 2015.
[3] S. R. Dabbagh, M. R. Sarabi, M. T. Birtek, S. Seyfi, M. Sitti, and S. Tasoglu, "3D-printed microrobots from design to translation," *Nature Commun.*, vol. 13, no. 1, 2022, Art. no. 5875.
[4] A. Aziz et al., "Medical imaging of microrobots: Toward in vivo applications," *ACS Nano*, vol. 14, no. 9, pp. 10865–10893, 2020.
[5] Z. Zhang, X. Wang, J. Liu, C. Dai, and Y. Sun, "Robotic micromanipulation: Fundamentals and applications," *Annu. Rev. Control, Robot., Auton. Syst.*, vol. 2, no. 1, pp. 181–203, 2019.
[6] B. J. Nelson, S. Gervasoni, P. W. Y. Chiu, L. Zhang, and A. Zemmar, "Magnetically actuated medical robots: An in vivo perspective," *Proc. IEEE*, vol. 110, no. 7, pp. 1028–1037, Jul. 2022.
[7] J. J. Abbott, E. Diller, and A. J. Petruska, "Magnetic methods in robotics," *Annu. Rev. Control, Robot., Auton. Syst.*, vol. 3, pp. 57–90, 2020.
[8] U. Bozuyuk, A. Aghakhani, Y. Alapan, M. Yunusa, P. Wrede, and M. Sitti, "Reduced rotational flows enable the translation of surface-rolling microrobots in confined spaces," *Nature Commun.*, vol. 13, no. 1, 2022, Art. no. 6289.
[9] M. M. Micheal, A. Adel, C.-S. Kim, J.-O. Park, S. Misra, and I.S.M Khalil, "2D magnetic actuation and localization of a surface milli-roller in low reynolds numbers," *IEEE Robot. Automat. Lett.*, vol. 7, no. 2, pp. 3874–3881, Apr. 2022.
[10] Y. Chen et al., "Carbon helical nanorobots capable of cell membrane penetration for single cell targeted sers bio-sensing and photothermal cancer therapy," *Adv. Funct. Mater.*, vol. 32, no. 30, 2022, Art. no. 2200600.
[11] V. Magdanz et al., "IRONSperm: Sperm-templated soft magnetic microrobots," *Sci. Adv.*, vol. 6, no. 28, 2020, Art. no. eaba5855.
[12] T. Xu, J. Zhang, M. Salehizadeh, O. Onaizah, and E. Diller, "Millimeter-scale flexible robots with programmable three-dimensional magnetization and motions," *Sci. Robot.*, vol. 4, no. 29, 2019, Art. no. eaav4494.
[13] Q. Ze et al., "Soft robotic origami crawler," *Sci. Adv.*, vol. 8, no. 13, 2022, Art. no. eabm7834.
[14] C. Huang, Z. Lai, X. Wu, and T. Xu, "Multimodal locomotion and cargo transportation of magnetically actuated quadruped soft microrobots," *Cyborg Bionic Syst.*, vol. 2022, 2022, Art. no. 0004.
[15] Z. Ren, W. Hu, X. Dong, and M. Sitti, "Multi-functional soft-bodied jellyfish-like swimming," *Nature Commun.*, vol. 10, no. 1, 2019, Art. no. 2703.
[16] A. Barbot, H. Tan, M. Power, F. Seichepine, and G.-Z. Yang, "Floating magnetic microrobots for fiber functionalization," *Sci. Robot.*, vol. 4, no. 34, 2019, Art. no. eaax8336.
[17] J. Lu, Y. Liu, W. Huang, K. Bi, Y. Zhu, and Q. Fan, "Robust control strategy of gradient magnetic drive for microrobots based on extended state observer," *Cyborg Bionic Syst.*, vol. 2020, 2022, Art. no. 9835014.
[18] M. Salehizadeh and E. Diller, "Three-dimensional independent control of multiple magnetic microrobots via inter-agent forces," *Int. J. Robot. Res.*, vol. 39, no. 12, pp. 1377–1396, 2020.
[19] O. Isitman, H. Kandemir, G. Alcan, Z. Cenev, and Q. Zhou, "Simultaneous and independent micromanipulation of two identical particles with robotic electromagnetic needles," in *Proc. IEEE Int. Conf. Manipulation, Automat. Robot. Small Scales*, 2022, pp. 1–6.
[20] F. N. Piñan Basualdo and S. Misra, "Collaborative magnetic agents for 3D microrobotic grasping,," *Adv. Intell. Syst.*, vol. 5, 2023, Art. no. 2300365.
[21] Z. Yang and L. Zhang, "Magnetic actuation systems for miniature robots: A review," *Adv. Intell. Syst.*, vol. 2, no. 9, 2020, Art. no. 2000082.
[22] M. C. Hoang et al., "Independent electromagnetic field control for practical approach to actively locomotive wireless capsule endoscope," *IEEE Trans. Syst., Man, Cybern. Syst.*, vol. 51, no. 5, pp. 3040–3052, May 2021.
[23] M. P. Kummer, J. J. Abbott, B. E. Kratochvil, R. Borer, A. Sengul, and B. J. Nelson, "OctoMag: An electromagnetic system for 5-DOF wireless micromanipulation," *IEEE Trans. Robot.*, vol. 26, no. 6, pp. 1006–1017, Dec. 2010.
[24] J. Sikorski, I. Dawson, A. Denasi, E. E. G. Hekman, and S. Misra, "Introducing BigMag–A novel system for 3D magnetic actuation of flexible surgical manipulators," in *Proc. IEEE Int. Conf. Robot. Automat.*, 2017, pp. 3594–3599.
[25] F. Ongaro, S. Pane, S. Scheggi, and S. Misra, "Design of an electromagnetic setup for independent three-dimensional control of pairs of identical and nonidentical microrobots," *IEEE Trans. Robot.*, vol. 35, no. 1, pp. 174–183, Feb. 2019.
[26] B. E. Kratochvil et al., "MiniMag: A hemispherical electromagnetic system for 5-DOF wireless micromanipulation," in *Proc. Exp. Robot.: 12th Int. Symp. Exp. Robot.*, 2014, pp. 317–329.
[27] J. Sikorski, S. Mohanty, and S. Misra, "MILIMAC: Flexible catheter with miniaturized electromagnets as a small-footprint system for microrobotic tasks," *IEEE Robot. Automat. Lett.*, vol. 5, no. 4, pp. 5260–5267, Oct. 2020.
[28] J. J. Huaroto et al., "MagNeed–needle-shaped electromagnets for localized actuation within compact workspaces," *IEEE Robot. Automat. Lett.*, vol. 8, no. 6, pp. 3908–3915, Jun. 2023.
[29] F. N. P. Basualdo et al., "Control and transport of passive particles using self-organized spinning micro-disks," *IEEE Robot. Automat. Lett.*, vol. 7, no. 2, pp. 2156–2161, Apr. 2022.
[30] J. Osborn, "Demagnetizing factors of the general elliysoitl," *Phys. Rev. Lett.*, vol. 67, pp. 11–12, 1945.
[31] M. Dkhil, M. Kharboutly, A. Bolopion, S. Régnier, and M. Gauthier, "Closed-loop control of a magnetic particle at the air–liquid interface," *IEEE Trans. Automat. Sci. Eng.*, vol. 14, no. 3, pp. 1387–1399, Jul. 2017.
[32] T. L. Thomas, J. Sikorski, G. K. Ananthasuresh, V. K. Venkiteswaran, and S. Misra, "Design, sensing, and control of a magnetic compliant continuum manipulator," *IEEE Trans. Med. Robot. Bionics*, vol. 4, no. 4, pp. 910–921, Nov. 2022.
[33] R. Hunt, Z. Zhao, E. Silver, J. Yan, Y. Bazilevs, and D. M. Harris, "Drag on a partially immersed sphere at the capillary scale," *Phys. Rev. Fluids*, vol. 8, Aug. 2023, Art. no. 084003.
[34] S. Salmanipour and E. Diller, "Eight-degrees-of-freedom remote actuation of small magnetic mechanisms," in *Proc. IEEE Int. Conf. Robot. Automat.*, 2018, pp. 3608–3613.
[35] E. Diller, J. Giltinan, G. Z. Lum, Z. Ye, and M. Sitti, "Six-degree-of-freedom magnetic actuation for wireless microrobotics," *Int. J. Robot. Res.*, vol. 35, no. 1–3, pp. 114–128, 2016.
[36] G. Lucarini, M. Mura, G. Ciuti, R. Rizzo, and A. Menciassi, "Electromagnetic control system for capsule navigation: Novel concept for magnetic capsule maneuvering and preliminary study," *J. Med. Biol. Eng.*, vol. 35, pp. 428–436, 2015.
[37] E. S. Gang et al., "Dynamically shaped magnetic fields: Initial animal validation of a new remote electrophysiology catheter guidance and control system," *Circulation: Arrhythmia Electrophysiol.*, vol. 4, no. 5, pp. 770–777, 2011.
[38] B. V. Johnson, N. Esantsi, and D. J. Cappelleri, "Design of the μmaze platform and microrobots for independent control and micromanipulation tasks," *IEEE Robot. Automat. Lett.*, vol. 5, no. 4, pp. 5677–5684, Oct. 2020.
[39] Y. Collard, F. N. Piñan Basualdo, A. Bolopion, M. Gauthier, P. Lambert, and N. Vandewalle, "Controlled transitions between metastable states of 2D magnetocapillary crystals," *Sci. Rep.*, vol. 12, no. 1, 2022, Art. no. 16027.